2020

Improving immunogenicity and safety of flagellin as vaccine carrier by high-density display on virus-like particle surface

Yiwen Zhao
University of Rhode Island

Zhuofan Li
University of Rhode Island

Xiaoyue Zhu
University of Rhode Island

Yan Cao
University of Rhode Island

Xinyuan Chen
University of Rhode Island, xchen14@uri.edu

Citation/Publisher Attribution

Zhao, Y., Li, Z., Zhu, X., Cao, Y., & Chen, X. (2020). Improving immunogenicity and safety of flagellin as vaccine carrier by high-density display on virus-like particle surface. *Biomaterials, 249*, 120030. doi: 10.1016/j.biomaterials.2020.120030
Available at: https://doi.org/10.1016/j.biomaterials.2020.120030

Improving immunogenicity and safety of flagellin as vaccine carrier by high-density display on virus-like particle surface

Yiwen Zhao, Zhuofan Li, Xiaoyue Zhu, Yan Cao, Xinyuan Chen*

Biomedical & Pharmaceutical Sciences, College of Pharmacy, University of Rhode Island, Kingston, RI

*Address Correspondence to: Xinyuan Chen, Biomedical & Pharmaceutical Sciences, College of Pharmacy, University of Rhode Island, Kingston, RI 02881, TEL: 401-874-5033; FAX: 401-874-5787; xchen14@uri.edu

The authors have no conflict of interest to declare.

Abstract
Flagellin is a protein-based adjuvant that activates toll-like receptor (TLR) 5. Flagellin has been actively explored as vaccine adjuvants and carriers. Preclinical and clinical studies find flagellin-based vaccines have a risk to induce systemic adverse reactions potentially due to its overt activation of TLR5. To improve safety and immunogenicity of flagellin as vaccine carriers, FljB was displayed at high densities on hepatitis b core (HBc) virus-like particle (VLP) surface upon c/e1 loop insertion. FljB-HBc (FH) VLPs showed significantly reduced ability to activate TLR5 or induce systemic interleukin-6 release as compared to FljB. FH VLPs also failed to significantly increase rectal temperature of mice, while FljB could significantly increase rectal temperature of mice. These data indicated systemic safety of FljB could be significantly improved by high-density display on HBc VLP surface. Besides improved safety, FH VLPs and FljB similarly boosted co-administered ovalbumin immunization and FH VLPs were found to induce two-fold higher anti-FljB antibody titer than FljB. These data indicated preserved adjuvant potency and improved immunogenicity after high-density display of FljB on HBc VLP surface. Consistent with the high immunogenicity, FH VLPs were found to be more efficiently taken up by bone marrow-derived dendritic cells (BMDCs) and stimulate more potent DC maturation than FljB. Lastly, FH VLPs were found to be a more immunogenic carrier than FljB, HBc VLPs, or the widely used keyhole limpet hemocyanin for nicotine vaccine development with good local and systemic safety. Our data support FH VLPs to be a potentially safer and more immunogenic carrier than FljB for vaccine development.

Keywords: Flagellin; FljB; TLR5; HBc; VLP; nicotine vaccine

Introduction

Flagellin is the major component of flagellar filament and has 4 structural domains (D0, D1, D2, and D3) [1]. D0/D1 domains form filament core and are composed of highly conserved N- and C-termini of flagellin [1]. D2/D3 domains form outer surface of filament and are composed of highly variable central region of flagellin [1]. Extracellular flagellin can be recognized by toll-like receptor (TLR) 5 and intracellular flagellin can be recognized by NOD-like receptor (NLR) family, apoptosis inhibitory protein 5 (NAIP5) to initiate NLR family CARD domain containing 4 (NLRC4) inflammasome activation [2, 3]. D1 domain contributes to TLR5 binding and filament formation and D0 domain contributes to NAIP5 recognition and NLRC4 inflammasome activation [4-6]. TLR5 binding leads to NFκB activation and release of pro-inflammatory cytokines, such as interleukin (IL)-6, while NLRC4 inflammasome activation leads to Caspase-1 activation [7].

Flagellin has been explored as vaccine adjuvants and carriers [8]. FljB and FliC from gram-negative Salmonella enterica serovar Typhimurium (*S. Typhimurium*) were actively explored for recombinant and conjugate vaccine development [9]. Foreign antigens can be co-administered with flagellin or inserted to its N- or C-terminus or highly variable D3 region to elicit potent immune responses [8]. Pre-existing immunity against flagellin showed no significant impacts on its adjuvant effects and potent adjuvant effects could be induced at relatively low doses prior to induction of maximal innate immunity [10, 11]. Despite these advantages, two flagellin-based influenza vaccines (VAX125 and VAX102) induced systemic adverse reactions especially at high doses in clinical studies [12, 13]. Both vaccines dose-dependently increased serum c-reactive protein (CRP) levels and some patients with systemic adverse reactions were accompanied with elevated serum IL-6 levels [12, 13]. Another flagellin-based influenza vaccine (VAX128) also dose-dependently increased serum CRP levels in old people and 4.8% subjects experienced at least 4-fold increase of serum IL-6 [14]. Increase of serum CRP and IL-6 levels were also observed in a recent clinical trial of a different flagellin-based influenza vaccine (VAX2012Q) [15]. Considering TLR5 activation leads to IL-6 secretion that in turn activates CRP release [12-15], over activation of TLR5 on various types of lymphoid and non-lymphoid cells may contribute to systemic adverse reactions associated with flagellin-based vaccines [8, 16].

Hepatitis b core protein (HBc) self-assembles into virus-like particles (VLPs) and c/e1 loop of HBc provides an ideal site for high-density display of antigenic epitopes on VLP surface [17-19]. Owing to its small size, short antigenic epitopes are preferred over full-length proteins for high-density display on HBc VLP surface upon c/e1 loop insertion. As of now, only two full-length proteins (green fluorescence protein (GFP, 238 aa) and outer surface protein C of the Lyme disease agent Borrelia burgdorferi (OspC, 189 aa)) with closely juxtaposed N- and C-termini were successfully displayed on HBc VLP surface via c/e1 loop insertion [20, 21]. Flagellin also has closely juxtaposed N- and C-termini based on its crystal structure (PDB code, 1UCU) and may be a good candidate for insertion into c/e1 loop of HBc without interference of its self-assembly into VLPs. High-density display of flagellin on HBc VLP surface may embed D0/D1 domains of flagellin in interior of VLPs and thus reduce its TLR5 activation ability and improve safety. At the same time, transition of flagellin from soluble to particulate form may increase its immunogenicity [22].

This study prepared high-density FljB-displayed HBc VLPs (FH VLPs) by insertion of full-length FljB (506 aa) into c/e1 loop of HBc. FH VLPs showed significantly reduced ability to activate TLR5 and induce systemic IL-6 release than FljB. FljB but not FH VLP immunization was found to significantly increase rectal temperature of mice. Besides improved safety, FH VLPs showed similar adjuvant effects to FljB in boosting co-administered ovalbumin (OVA) immunization and FH VLPs induced more than two-fold higher anti-FljB antibody titer and FljB. Consistent with improved immunogenicity, FH VLPs could be more efficiently taken up by bone marrow-derived DCs (BMDCs) and stimulate more potent BMDC maturation than FljB. Lastly, we found FH VLPs were a more immunogenic carrier than FljB, HBc VLPs, and the widely used keyhole limpet hemocyanin (KLH) for nicotine vaccine development.

Materials and methods

Reagents

All enzymes used in molecular cloning experiments were purchased from New England Biolabs (Ipswich, MA). Fluorescence-conjugated antibodies used in immunostaining and flow cytometry were purchased from Biolegend (San Diego, CA) or Thermo Fisher Scientific (Waltham, MA). HEK-Blue™ mTLR5 cell line (hkb-mtlr5) and flagellin control (FLA-ST, Ultrapure) were purchased from Invivogen (San Diego, CA). Recombinant murine granulocyte macrophage colony-stimulating factor (GM-CSF, 415-ML/CF) and IL-4 (404-ML/CF) were purchased from R & D Systems (Minneapolis, MN). CpG 1826 was synthesized by Trilink Biotechnologies (San Diego, CA). 8-well chamber slides (Nunc™ Lab-Tek™ Chamber Slide™, 177442), LysoTracker™ Deep Red (L12492), Hoechst 33342 (H1399), RIPA buffer (89900), protease and phosphatase inhibitor cocktail (78442), Alum (Imject Alum, 77161), KLH (Imject mcKLH, 77600), bovine serum albumin (BSA, Imject, 77110) were purchased from Thermo Fisher Scientific (Waltham, MA). Antifade fluorescence mounting medium (ab104135) was purchased from Abcam (Cambridge, MA).

Animals

BALB/c and C57BL/6 mice (male, 6-8 weeks old) were purchased from Charles River Laboratories (Wilmington, MA). MyD88 knockout (KO) mice were purchased from Jackson Laboratory (Bar Harbor, ME) and self-bred for use in this study. Animals were housed in animal facilities of University of Rhode Island. Mice were anesthetized by intraperitoneal injection of ketamine (80 mg/kg) and xylazine (10 mg/kg) for hair removal and intradermal (ID) immunization. All animal procedures were approved by Institutional Animal Care and Use Committee of University of Rhode Island.

Recombinant plasmid construction

FljB gene of *S. Typhimurium strain LT2* and partial HBc gene encoding 1-149 region of *adw* subtype were synthesized by Thermo Fisher Scientific. Forward primer (5'-GCGCATATGGGCAGCAGC*CATCATCATCATCATCAC* AGCAGCGGC*CTGGTGCCGCGCGGCAGC*GCACAAGTAATCAAC-3') containing Nde I recognition site (underlined), his-tag sequence (italicized), and thrombin cleavage site (underlined and italicized) and reverse primer (5'-GCGCTCGAG*TTA*ACGTAACAGAGAC AGCACG-3') containing Xho I recognition site (underlined) and stop codon (italicized) were used to amplify FljB gene. Forward primer (5'-GCGCATATGGACATTGACCCGTATA AAG-3') containing Nde I recognition site (underlined) and reverse primer (5'-GCGCTCGAG AACAACAGTAGTTTCCGG-3') containing Xho I recognition site (underlined) were used to amplify HBc (1-149) gene. Polymerase chain reaction (PCR) products of FljB and HBc genes were subjected to Xho I and Nde I digestion and then ligated into pET-29a vector digested with the same enzymes.

Overlapping PCR was used to insert FljB gene into c/e1 loop of HBc (A80-S81), as illustrated in Fig.1B. A flexible linker GGGGSGGGGS or $(G_4S)_2$ was inserted between HBc and FljB sequences to increase protein chain flexibility during refolding. In more detail, the aforementioned forward primer of HBc and reverse primer (5'-TGCTGGATCTTCCAAATTA CTTCCCACC-3') were used to amplify HBc (1-80), forward primer (5'- GGTGGGAAGTA ATTTGGAAGATCCAGCA*GGTGGTGGTGGTAGTGGTGGTGGTGGTAGT* GCACAAGT

AATCAACACTAACAGT-3') containing overlapping sequence to reverse primer of HBc (underlined), linker sequence (italicized), and N-terminal FljB sequence (no formatting), and reverse primer (5'-ACGTAACAGAGACAGCACGTTCTGCGGG-3') were used to amplify FljB gene. Forward primer (5'-CCCGCAGAACGTGCTGTCTCTGTTACGT*GGTGGTGG TGGTAGTGGTGGTGGTGGTAGT*TCCCGGGAATTAGTAGTCAGCTATGTC-3') containing overlapping sequence to reverse primer of FljB gene (underlined), linker sequence (italicized), and HBc (81-89) sequence (no formatting), and the aforementioned reverse primer of HBc were used to amplify HBc (81-149) gene. The above 3 PCR products were mixed at 1:1:1 molar ratio and allowed to anneal and extend. Forward and reverse primers of HBc (1-149) were used to amplify FljB-HBc gene sequence and PCR products were purified, digested with Xho I and Nde I, and ligated into pET-29a vector. Successful ligation was confirmed with sequencing after transformation of ligated pET-29a vector into competent DH5α cells.

Expression and purification of FljB-HBc, FljB, and HBc

Bacterial BL21 cells were transformed with FljB-HBc, FljB, and HBc plasmids after sequence confirmation and grown in LB medium. Overnight bacteria culture was diluted 1:100 in fresh LB medium and grown to OD_{600nm} reaching 0.8-1.0. Isopropyl-β-D-thiogalactoside (IPTG) was added to stimulate protein expression. Bacteria cells were harvested 3 hours later and centrifuged. Bacteria pellets were resuspended in lysis buffer (50 mM Tris-HCl, 300 mM NaCl, pH 8.0) followed by sonication and centrifugation. Supernatants were used to purify FljB under native condition, while inclusion bodies were used to purify FljB-HBc and HBc under denatured conditions. In more detail, supernatants from FljB-expressing bacteria were loaded onto a Ni-NTA column, washed, and eluted with 0.3 M imidazole. Inclusion bodies from HBc and FljB-HBc-expressing bacteria were washed and dissolved in above lysis buffer supplemented with 8M Urea. After centrifugation, supernatants were loaded onto a Ni-NTA column, washed, and eluted with 0.3 M imidazole. FljB samples were dialyzed against phosphate-buffered saline (PBS), while HBc and FljB-HBc samples were dialyzed against PBS with reducing Urea concentrations (4, 2, and 0 M). FljB was subjected to thrombin cleavage to remove N-terminal his-tag via Thrombin CleanCleave™ Kit (RECOMT-1KT, Sigma). Purified proteins were subjected to SDS-PAGE analysis. Soluble proteins in FljB-HBc and HBc samples were removed by size-exclusion column loaded with Sepharose CL-4B (17015001, GE Healthcare Life Science).

Transmission electron microscopy (TEM)

For negative staining TEM, FH VLP and HBc VLP samples were deposited on carbon/Formvar-coated copper grids (01813-F, Ted Pella, Redding, CA) and then negatively stained with 2% uranyl acetate (22400, Electron Microscopy Sciences, Hatfield, PA). For immunogold labeling TEM, HBc VLPs and FH VLPs were deposited on carbon/Formvar-coated copper grids and then blocked with PBS supplemented with 1% BSA (blocking buffer). After that, VLP-deposited grids were incubated with 1:10 diluted anti-FljB antiserum or non-immune serum and then washed 3 times in blocking buffer. Grids were then incubated with 1:20 diluted 6 nm gold-conjugated goat-anti-mouse secondary antibody (25123, Electron Microscopy Sciences, Hatfield, PA). After 3 times of wash in blocking buffer and 3 times of wash in water, grids were negatively stained with 2% uranyl acetate. TEM images were acquired with a JEM-2100F electron microscope (JEOL, Peabody, MA) at 200 kV.

TLR5 activation assay

Murine TLR5 and an inducible SEAP (secreted embryonic alkaline phosphatase) reporter gene-co-transfected HEK293 cells (HEK-Blue™ mTLR5 cell line) were used to explore TLR5 activation ability of FH VLPs following Manufacturer's instructions. In brief, after cells reached ~80% confluency, cells were harvested, adjusted to 140,000 cells/mL using HEK-Blue™ detection medium that contained a specific SEAP color substrate to facilitate the detection, and then seeded into 96-well plates (180 µl/well). FH VLPs, FljB, FLA-ST, and HBc VLPs were added at final concentrations of 8, 40, 200, 1000 pM. Cells were incubated for 10 hours and OD_{620nm} was read in a microplate reader to indicate relative TLR5 activation ability.

Western Blotting

Purified FljB-HBc, FljB, and HBc were subjected to western blotting analysis. In brief, proteins (10-50 ng) were separated in SDS-PAGE and then transferred to PVDF membrane. After blocking with 5% non-fat milk in TBST (Tris-buffered saline (TBS)/0.1% Tween 20, pH 7.6), PVDF membrane was incubated with 1:1000 diluted anti-FljB or anti-HBc antiserum in blocking buffer for 90 minutes. After 3 times of wash in TBST, PVDF membrane was incubated with horseradish peroxidase (HRP)-conjugated horse-anti-mouse secondary antibody (7076S, Cell Signaling Technology). After 3 times of wash in TBST, SuperSignal™ West Femto Maximum Sensitivity Substrate (34095, Thermo Fisher Scientific) was added and myECL imager (Thermo Fisher Scientific) was used for chemiluminescent imaging. To detect mature Caspase-1 p20 band, stimulated BMDCs were lysed in RIPA buffer supplemented with protease and phosphatase inhibitor cocktail. The same amount of proteins in each group were separated in SDS-PAGE and then transferred to PVDF membrane. After blocking, PVDF membrane was incubated with 1 µg/mL mouse anti-Caspase-1 (p20) antibody (AG-20B-0042, Adipogen Life Sciences) followed by the same procedures as described above to detect Caspase-1 p20 subunit. To detect GAPDH expression, PVDF membrane was stripped in stripping buffer (62.5 mM Tris-HCl, 2% SDS, 0.7% β-mercaptoethanol, pH 6.8) at 50˚C for 30 minutes. PVDF membrane was then incubated with rabbit anti-GAPDH antibody (D16H11, 5174S, Cell Signaling Technology) and HRP-conjugated goat-anti-rabbit secondary antibody (7074P2, Cell Signaling Technology) for GAPDH detection.

Fluorescent dye conjugation

Alexa Fluor 555 (AF555) was conjugated to FH VLPs, FljB, and HBc VLPs with AF555 NHS Ester (AF555, Invitrogen) based on Manufacturer's instructions. In brief, AF555 was dissolved in DMSO at 10 mg/ml and 20 µl AF555 was added to 1 mg FH VLPs, FljB, and HBc VLPs in 100 µl PBS. After 1 hour of reaction at room temperature, free AF555 was removed by dialysis against PBS.

Antigen uptake and maturation of DCs

Bone marrow was isolated from femur and tibia of C57BL/6 mice and cultured in the presence of recombinant murine GM-CSF (15 ng/ml) and IL-4 (10 ng/ml) as in our previous report [23]. Non-adherent immature BMDCs were harvested on day 6 and seeded at 1×10^6 cells/mL into 8-well chamber slides. AF555-conjugated FH VLPs, FljB, and HBc VLPs were added at a final concentration of 70 nM of respective proteins. LysoTracker™ Deep Red (75 nM) was added 1.5 hours later to stain acidic organelles and Hoechst 33342 (2 µg/mL) was added 2.5 hours later to stain cell nuclei. Cells were washed with PBS for 3 times at 3 hours and then fixed in 4% paraformaldehyde for 20 minutes. After removal of chamber wells, chamber slides were

mounted with antifade fluorescence mounting medium followed by confocal imaging under Nikon Eclipse Ti2 inverted confocal microscope. For flow cytometry analysis, BMDCs were seeded at 1×10^6 cells/mL in 96-well plates and then incubated with AF555-conjugated FH VLPs, FljB, and HBc VLPs at the above concentration. Cells were harvested 3 and 20 hours later, stained with fluorescence-conjugated anti-CD11c (N418), and then subjected to flow cytometry analysis of percentage of $AF555^+$ cells in $CD11c^+$ cells in BD FACSVerse. For maturation study, immature BMDCs were seeded at the same concentration to 96-well plates and stimulated with FH VLPs, FljB, and HBc VLPs at the above concentration for 20 hours. Cells were stained with fluorescence-conjugated anti-CD11c (N418), anti-CD40 (3/23), anti-CD80 (16-10A1), and anti-CD86 (GL-1) followed by flow cytometry analysis of surface expression of CD40, CD80, and CD86 in BD FACSVerse. To explore whether FH VLPs stimulated *in vivo* DC maturation, 5 μg FH VLPs, 3.7 μg FljB, and 1.2 μg HBc VLPs (equal moles) were intradermally injected into lateral back skin of C57BL/6 mice. Skin was dissected 24 hours later and single-cell suspensions were prepared as in our previous report [24]. Skin cells were then similarly stained with fluorescence-conjugated anti-CD11c, anti-CD40, anti-CD80, and anti-CD86 followed by flow cytometry analysis as above.

Immunization

To explore adjuvant effects of FH VLPs and FljB, BALB/c mice were intradermally immunized with 10 μg OVA alone or in the presence of 3 μg FH VLPs or 2.2 μg FljB (same mole). Immunization was repeated 3 weeks later. To compare relative immunogenicity of FH VLPs and FljB to induce anti-FljB antibodies and impacts of MyD88 on anti-FljB antibody production, wild type (WT) and MyD88 KO mice were intradermally immunized with 5.0 μg FH VLPs or 3.7 μg FljB (same mole). Immunization was repeated 3 weeks later. To compare relative immunogenicity of FljB-Nic to KLH-Nic, BALB/c mice were intradermally immunized with 3 μg FljB-Nic or KLH-Nic. To compare relative immunogenicity of HBc-Nic to KLH-Nic, BALB/c mice were intradermally immunized with 3 μg HBc-Nic or KLH-Nic. To compare relative immunogenicity of FH-Nic to KLH-Nic and whether chemical adjuvants could boost FH-Nic immunization, BALB/c mice were intradermally immunized with 3 μg FH-Nic in the presence or absence of Alum (1:1 volume ratio), 30 μg CpG 1826, or combinatorial CpG/Alum adjuvant, or intradermally immunized with 3 μg KLH-Nic or left non-immunized. Adjuvants were simply mixed with vaccines before delivery in this study. Immunization was repeated three times at a 3-week interval.

Serum antibody titer

A small volume of blood (25-50 μl) was collected 3 weeks after immunization. Serum antibody titer was measured by enzyme-linked immunosorbent assay (ELISA) by coating 1 μg/ml FljB, HBc VLPs, or BSA-conjugated nicotine (BSA-Nic) onto 96-well ELISA plates as in our previous report [25]. For detection of isotype IgG1 and IgG2a or IgG2c antibody titer, HRP-conjugated anti-mouse IgG1, IgG2a or IgG2c secondary antibodies were used.

Cytokine levels

Serum IL-6 levels were measured by Mouse IL-6 ELISA Ready-SET-Go kit (88-7064-88, eBioscience). Supernatant IL-12 levels were measured by Mouse IL-12 p70 ELISA Ready-SET-Go kit (50-172-51, eBioscience).

Nicotine challenge and tissue nicotine detection
Mice were weighed and intravenously challenged with 0.03 mg/kg nicotine. Five minutes later, brain and trunk blood were collected, and tissue nicotine was extracted following methods established by Pentel et. al. [26]. Brain and serum nicotine levels were quantified by gas chromatography-mass spectrometry and expressed as nicotine amount per gram of brain or per milliliter of serum as in our previous report [25].

Endotoxin removal
Endotoxin in FH VLPs, FljB, and HBc VLPs was removed by a commercial endotoxin-removal column (20344, Thermo Fisher Scientific) or Pierce™ High Capacity Endotoxin Removal Resin (88270, Thermo Fisher Scientific) according to Manufacturer's Instructions. Remaining endotoxin levels were quantified by Pierce™ LAL Chromogenic Endotoxin Quantitation Kit (88282, Thermo Fisher Scientific) or Pierce™ Chromogenic Endotoxin Quant Kit (A39552, Thermo Fisher Scientific) and found to be below 2.5 ng/mg.

Nicotine hapten conjugation
Conjugation of nicotine hapten (CMUNic) to FH VLPs, FljB, HBc VLPs, KLH, and BSA referred to our previous study [25]. In brief, 1 mg CMUNic was activated with 5 mg *N*-(3-dimethylaminopropyl)-*N′*-ethylcarbodiimide hydrochloride (EDAC, E1769, Sigma) at room temperature for 10 minutes. FH VLPs, FljB, HBc VLPs, KLH, and BSA (1 mg) was added to the above mixture and kept at room temperature for 3 hours with continuous stirring. Nicotine conjugates were then dialyzed against PBS for 3 times.

Antibody avidity index
Seram samples were individually analyzed for antibody avidity by competitive ELISA as reported [27]. In brief, serum samples were subjected to 10-fold serial dilutions and added to 96-well plates coated with BSA-Nic. After 90 minutes of incubation, NH_4SCN (2M) was added to elute loosely bound antibody. ELISA plates were then incubated with HRP-conjugated sheep-anti-mouse secondary antibody (NA931, GE Healthcare Life Sciences) followed by addition of TMB substrate. Reactions were stopped by 3M H_2SO_4 and OD_{450nm} was read in a microplate reader. OD_{450nm} against log dilutions of immune sera was plotted in the presence or absence of NH_4SCN. Areas under the curve were then calculated. Ratio of the area under the curve in the presence versus absence of NH_4SCN was calculated and used as antibody avidity.

Statistics
Values were expressed as Mean ± SEM (standard error of the mean). Student's t-test was used to compare differences between groups. One-way analysis of variance (ANOVA) with Tukey's or Bonferroni's multiple comparison test was used to compare differences for more than two groups or otherwise specified. P value was calculated by PRISM software (GraphPad, San Diego, CA) and considered significant when it was less than 0.05.

Results

FljB-HBc self-assembles into VLPs

C/e1 loop of HBc provides an ideal site for insertion of foreign antigens for display on VLP surface [17-19]. As shown in Fig.1A, c/e1 loop of HBc is localized in the flexible region of two α-helices and form the tip of spikes on VLP surface. N- and C-termini of *S. Typhimurium* FliC is proximate to each other based on its crystal structure (Fig.1A). *S. Typhimurium* FljB shares high N- and C-terminal homology with FliC (Suppl. Fig.1) and is expected to also have closely juxtaposed N- and C-termini. As of such, insertion of FljB into c/e1 loop of HBc is less likely to pose significant steric hindrance to self-assembly of HBc into VLPs, thus allowing high-density display of FljB on HBc VLP surface, as depicted in Fig.1A. DNA was constructed to express full-length FljB between A80 and S81 of c/e1 loop of HBc and $(G_4S)_2$ linker was inserted between FljB and HBc sequences to increase protein chain flexibility (Fig.1B). Recombinant FljB-HBc, FljB, and HBc with a theoretical molecular weight of 71.3, 52.5, and 17.7 kDa, respectively, were expressed in *E. coli*, purified, refolded, and analyzed by SDS-PAGE (Fig.1C). Western blotting analysis confirmed the presence of both FljB and HBc in FljB-HBc fusion protein. As shown in Fig.1D, FljB-HBc and FljB but not HBc samples showed positive bands at the right position when PVDF membrane was blotted with anti-FljB antiserum. As shown in Fig.1E, FljB-HBc and HBc but not FljB samples showed positive bands at the right position when PVDF membrane was blotted with anti-HBc antiserum.

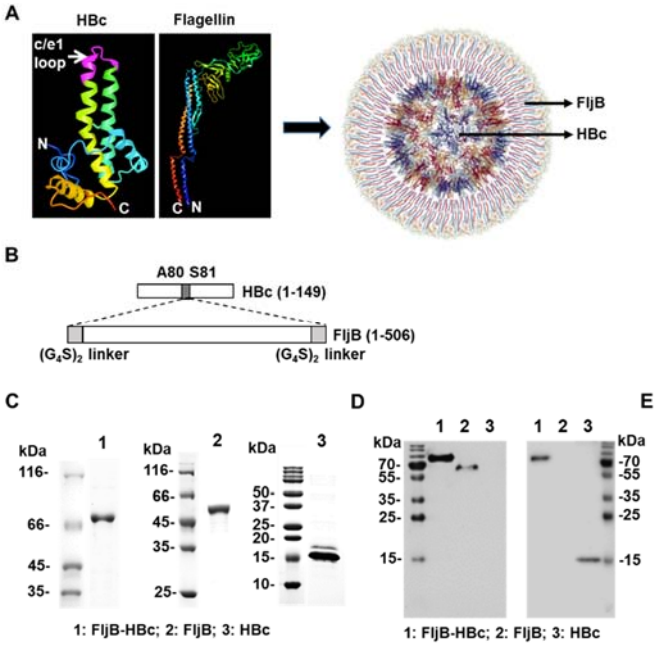

Fig.1 Expression and characterization of recombinant FljB-HBc, FljB and HBc

A. Crystal structure of HBc and Flagellin in web-based 3D structure viewer (iCN3D) and depict of high-density FljB-displayed HBc VLPs. Protein data bank (PDB) codes used were 1QGT (HBc) and 1UCU (FliC). C/e1 loop (N74-L84) of HBc was highlighted in magenta. N- and C-termini of HBc and FljB were labeled with letter N and C, respectively. **B**. Schematic of DNA construct for FljB-HBc fusion protein expression. Full-length FljB (1-506) flanked with $(G_4S)_2$ linkers was inserted between A80 and S81 of c/e1 loop of HBc (1-149, *Adw* subtype). **C**. Recombinant FljB-HBc, FljB, and HBc were subjected to SDS-PAGE analysis. **D-E**. Recombinant FljB-HBc, FljB, and HBc were subjected to western blotting analysis. Anti-FljB

antiserum was used to blot PVDF membrane in **D** and anti-HBc antiserum was used to blot PVDF membrane in **E**.

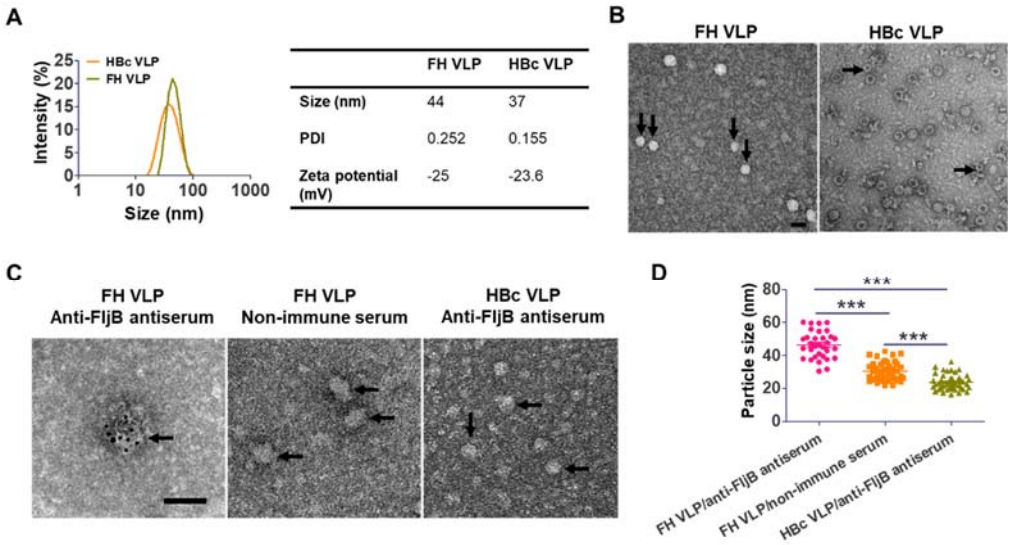

	FH VLP	HBc VLP
Size (nm)	44	37
PDI	0.252	0.155
Zeta potential (mV)	-25	-23.6

Fig.2 Characterization of FH VLPs and HBc VLPs

A. DLS and zeta potential measurements of FH and HBc VLPs. Particle size distributions were shown in the left. Particle size, PDI, and zeta potential were listed on the right. **B**. Representative TEM images of FH and HBc VLPs following negative staining. Arrows point to clearly small particles. Scale: 50 nm. **C**. Representative TEM images of FH VLPs following immunogold staining with anti-FljB antiserum (left) or non-immune serum (middle) or HBc VLPs following immunogold staining with anti-FljB antiserum (right). Arrows point to VLPs. Scale: 50 nm. **D**. Particle size of FH and HBc VLPs after immunogold staining in **C** was measured in Image J (n=32-46). One-way ANOVA with Tukey's multiple comparison test was used to compare differences between groups in **D**. ***: $p<0.001$.

Next, FljB-HBc and HBc samples were subjected to dynamic light scattering (DLS) analysis in Zetasizer Nano ZS (Malvern). As shown in Fig.2A, FH and HBc VLPs had a size of 44 and 37 nm, respectively, with a PDI value less than 0.3 for both particles. Zeta potential was also measured and found to be -25 mV for FH VLPs and -23.6 mV for HBc VLPs at neutral pH (Fig.2A), in line with the theoretical isoelectric point (pI) of 5.03 and 5.73 for FljB-HBc and HBc, respectively (ExPASy). Slightly more net negative charge of FH VLPs can be explained by the slightly lower pI of FljB-HBc. TEM analysis found both samples contained round-shaped particles less than 50 nm in diameter (Fig.2B). We further found HBc and FH VLPs contain two particle sizes, in line with report that HBc could self-assemble into particles with two icosahedral symmetries (T = 3 and T = 4) [28]. T = 3 and T = 4 particles contain 180 and 240 copies of HBc, respectively, with T =3 particles slightly smaller than T =4 particles [28]. More details about assembling symmetry of FH VLPs remain to be explored with high-resolution cryo-electron microscope or scanning transmission electron microscope [28]. As compared to HBc VLPs, FH VLPs showed brighter signals following negative staining and TEM, which may be caused by reduced scattering of electron beams due to dense FljB coating [29].

We further conducted immunogold labeling TEM to verify the presence of FljB on FH VLP surface. As shown in Fig.2C, FH VLPs showed positive immunogold signals after staining with anti-FljB antiserum but not non-immune serum. As a negative control, HBc VLPs showed no immunogold signals after immunogold staining with anti-FljB antiserum (Fig.2C). These results clearly indicated the presence of FljB on HBc VLP surface. We further measured particle size of the different VLPs after immunogold labeling. As shown in Fig.2D, FH VLPs had a size of 46 nm after immunogold staining with anti-FljB antiserum and a size of only 30 nm after immunogold staining with non-immune serum. Such a difference is likely to be caused by the immunogold staining that revealed FljB on FH VLP surface. Interestingly, the distance between Leu493 (end of D0 domain) and Ala184 (middle of the D2/D3 domain) of FliC was about 15 nm (Suppl. Fig.2), which matched very well with the above size difference. HBc VLPs had a size of 24 nm after immunogold staining with anti-FljB antiserum (Fig.2D). In TEM studies without immunogold staining, we failed to observe spikes on FH VLP surface, while spikes were found in outer surface protein C-displayed HBc VLP surface [21]. This may simply reflect the resolution difference of electron microscope equipment. Immunogold labeling TEM revealed surface-displayed FljB and allowed us to more accurately measure FH VLP size, which was much bigger than HBc VLPs (Fig.2D). High-resolution TEM or cryo-EM would be needed to reveal the ultrafine surface structure of FH VLPs.

Impaired TLR5 and Caspase 1 activation while preserved adjuvant effects

FljB activates both TLR5 and NLRC4 inflammasome. The ability of FH VLPs to activate TLR5 and NLRC4 inflammasome was then explored and compared with FljB and FLA-ST. FLA-ST is ultrapure FliC purified from *S. Typhimurium* based on manufacturer's description. HEK293 cells co-transfected with murine TLR5 and SEAP reporter gene were incubated with FH VLP, FljB, and FLA-ST at different molar concentrations of respective proteins. As shown in Fig.3A, FH VLPs showed much weakened ability to activate TLR5 than FljB and FLA-ST. The lowest concentration of FljB, FLA-ST, and FH VLPs to significantly activate TLR5 was 8, 40, and 1000 pM, respectively (Fig.3A), indicating 25-fold reduced TLR5 activation ability of FH VLPs as compared to FLA-ST and more than 100-fold reduced TLR5 activation ability of FH VLPs as compared to FljB. Next, the ability of FH VLPs to activate NLRC4 inflammasome was explored. NLRC4 inflammasome is a multi-protein complex, the activation of which cleaves pro-Caspase-1 to form p10/p20 heterodimer. Here we directly analyzed Caspase-1 activation following incubation of BMDCs with FH VLPs, FljB, and FLA-ST to reflect their NLRC4 inflammasome activation ability. As shown in Fig.3B, Caspase-1 p20 subunit could be readily detected after BMDC incubation with FljB and FLA-ST but not FH VLPs. This result indicated significant loss of NLRC4 inflammasome activation ability of FH VLPs.

Considering FljB doesn't require strong activation of innate immunity to exert its adjuvant effects, we explored adjuvant effects of FH VLPs on boosting co-administered OVA immunization in BALB/c mice. As shown in Fig.3C, FH VLPs but not FljB significantly increased anti-OVA antibody titer after prime. FH VLPs also similarly increased anti-OVA antibody titer to FljB after boost (Fig.3D). To explore whether adjuvant effects of FH VLPs could be observed in another species of mice and whether FH VLPs could dose-dependently increase OVA-induced antibody production, C57BL/6 mice were intradermally immunized with OVA alone or in the presence of increasing FH VLP doses (3, 10, and 30 μg). As shown in Suppl. Fig.3A, low dose but not medium or high dose of FH VLPs significantly increased anti-

OVA antibody titer in C57BL/6 mice. Furthermore, low-dose FH VLPs more significantly increased anti-OVA IgG2c antibody titer than IgG1 antibody titer (Suppl. Fig.3B-C). Mouse immunization studies indicated FH VLPs possessed potent adjuvant effects despite the lack of significant TLR5 and NLRC4 inflammasome activation abilities.

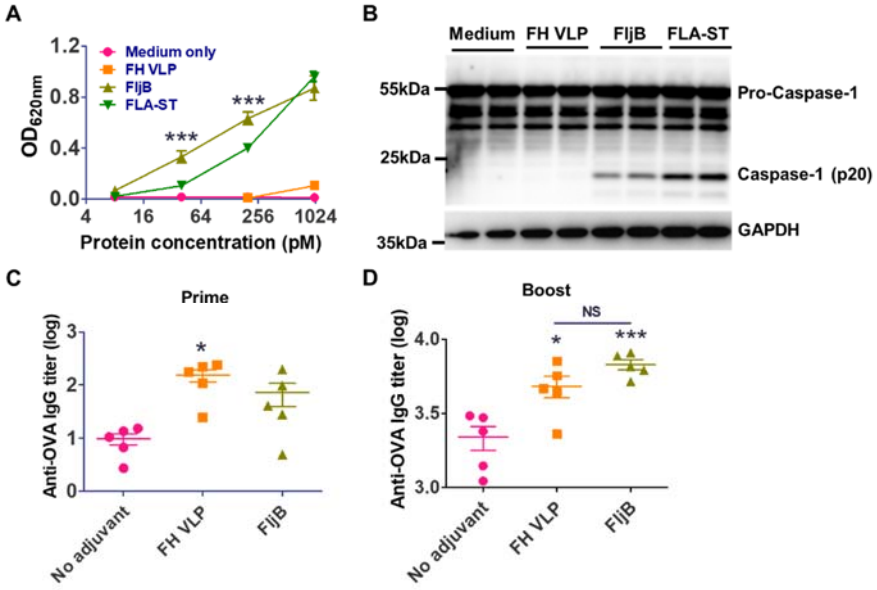

Fig.3 Impaired TLR5 and Caspase 1 activation of FH VLPs

A. TLR5 activation ability of FH VLPs, FljB, and FLA-ST. HEK293 cells co-transfected with TLR5 and SEAP reporter gene were incubated with FH VLPs, FljB, and FLA-ST in triplicate at 8, 40, 200, 1000 pM of respective proteins to keep equal flagellin contents across groups at each treatment concentration. OD_{620nm} was read 10 hours later to indicate relative TLR5 activation ability. **B**. Caspase-1 activation ability of FH VLPs, FljB, and FLA-ST. BMDCs were incubated with FH VLPs, FljB, and FLA-ST at 70 nM of respective protein levels in duplicate for 24 hours. Expression of pro-Caspase-1, Caspase-1 (p20), and house-keeping gene GAPDH was analyzed by western blotting. **C-D**. BALB/c mice were intradermally immunized with 10 µg OVA alone or in the presence of 3 µg FH VLPs or FljB. Immunization was repeated 3 weeks later. Serum anti-OVA antibody titer was measured 3 weeks after prime (**C**) and boost (**D**). Two-way ANOVA with Bonferroni's post-test was used to compare differences between groups at each protein concentration in **A**. One-way ANOVA with Tukey's multiple comparison test was used to compare differences between groups in **C** and **D**. n=5 in **C** and **D**. *: $p<0.05$; ***: $p<0.001$. NS: not significant.

More efficient uptake of FH VLPs than FljB by BMDCs

Good vaccine carriers need to be efficiently taken up by antigen presenting cells (APCs). Uptake of FH VLPs and FljB was then explored in BMDCs. Soluble proteins are often endocytosed and sorted through early endosomes, late endosomes, and lysosomes[30]. Particulate antigens are often phagocytosed and end up in phagolysosomes formed by fusion of phagosomes and lysosomes[30]. Considering lysosomes and phagolysosomes have a pH of 4-4.5 [30], LysoTracker capable of staining acidic organelles was used to stain both structures in this study. BMDCs were incubated with AF555-conjugated FH VLPs, FljB, and HBc VLPs at equal molar concentrations of respective proteins. FH VLPs showed more significant uptake than FljB as evidenced by much stronger AF555 signals in FH VLP group than FljB group (Antigen, Fig.4A).

We further found the majority of AF555 signals in both FH VLP and FljB groups overlapped with LysoTracker signals (Merged, Fig.4A). HBc VLPs were also included for comparison and we found BMDCs could also significantly take up HBc VLPs into lysosomes (Fig.4A). BMDC uptake of FH VLPs, FljB, and HBc VLPs at equal molar concentrations was also explored by flow cytometry. As shown in Fig.4B-C, percentage of $AF555^+$ DCs was 25% in FH VLP group, 19% in HBc VLP group, 8% in FljB group, and less than 1% in medium only group. Percentage of $AF555^+$ DCs was significantly higher in FH VLP group than that in FljB group (Fig.4C). Percentage of $AF555^+$ DCs was also significantly higher in FH VLP group than that in HBc VLP group (Fig.4C). The same trend was also observed at 20 hours of incubation (Fig.4D). The same experiment was repeated by incubation of BMDCs with equal fluorescence intensities of FH VLPs, FljB, and HBc VLPs, equivalent to ~1:2:5 molar concentrations of FljB-HBc, FljB, HBc. We still observed significantly increased uptake of FH VLPs as compared to soluble FljB although HBc VLPs showed the most significant uptake this time (Suppl. Fig.4). These data indicated FH VLPs could be more efficiently taken up by BMDCs than FljB.

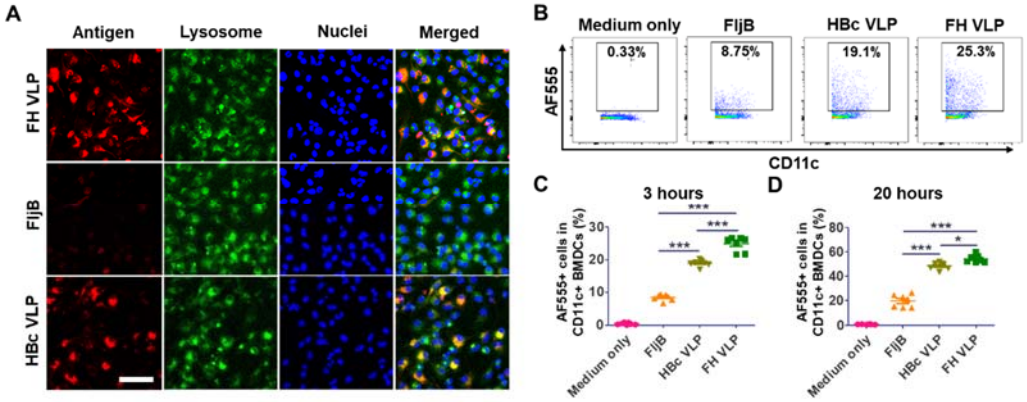

Fig.4 More efficient uptake of FH VLPs than FljB

A. BMDCs were incubated with AF555-labeled FH VLPs, FljB, and HBc VLPs at equal molar concentrations (70 nM) of respective proteins, equivalent to ~5:2.5:1 fluorescence intensity, in 8-well chamber slides. LysoTracker and Hoechst 33342 were added 1.5 and 2.5 hours later. Cells were subjected to fluorescence confocal imaging 3 hours later. Scale: 50μm. **B-D**. BMDCs were incubated with AF555-labeled FH VLPs, FljB, and HBc VLPs as in A in 96-well plates. Cells were harvested 3 and 24 hours later, stained with fluorescence-conjugated anti-CD11c followed by flow cytometry analysis. Cells were first gated based on SSC and FSC and then based on CD11c expression. Representative dot plots of percentage of $AF555^+$ DCs at 3 hours were shown in **B**. Percentage of $AF555^+$ DCs at 3 and 20 hours was shown in **C** and **D**, respectively. n=5. One-way ANOVA with Tukey's multiple comparison test was used to compare differences between groups. *: $p<0.05$; ***: $p<0.001$. Experiments were repeated twice with similar results.

FH VLPs stimulate more potent DC maturation than FljB

Besides efficient uptake, stimulation of DC maturation by vaccine carriers is also crucial to elicit potent vaccine-specific immune responses. We then explored the relative ability of FH VLPs to stimulate BMDC maturation to FljB, FLA-ST, and HBc VLPs. In brief, BMDCs were stimulated with FH VLPs, FljB, FLA-ST, and HBc VLPs at equal molar concentrations of respective proteins. Surface expression of costimulatory molecules CD40, CD80, and CD86 was explored 20 hours later. We found BMDCs could be divided into two populations based on CD40 expression: $CD40^{high}$ ($CD40^{hi}$) and $CD40^{low}$ ($CD40^{lo}$), as shown in Fig.5A. MFI of CD40, CD80,

and CD86 was compared among groups. We found MFI of CD40 was significantly increased in FH VLP group but not in FljB, FLA-ST, or HBc VLP group when compared to that in medium only group (Fig.5B). MFI of CD40 in FH VLP group was also significantly higher than that in FljB, FLA-ST, and HBc VLP group (Fig.5B). FH VLPs and FLA-ST slightly increased MFI of CD80 and CD86 (Fig.5C-D). MFI of CD80 and CD86 in FH VLP and FLA-ST groups was significantly higher than that in HBc VLP group but not medium only group (Fig.5C-D). MFI of CD86 in FljB group was also significantly higher than that in HBc VLP group (Fig.5D). Next, we compared percentage of $CD40^{hi}$, $CD80^{hi}$, and $CD86^{hi}$ DCs among the different groups. We found percentage of $CD40^{hi}$, $CD80^{hi}$, and $CD86^{hi}$ DCs was significantly higher in FLA-ST group than HBc VLP group and percentage of $CD40^{hi}$ DCs was significantly higher in FH VLP group than HBc VLP group (Fig.5E-G). The above results indicated FH VLPs were the most potent stimulator to increase surface expression of costimulatory molecules, among which CD40 expression showed the most significant increase. Although FH VLPs could stimulate BMDC maturation, the ability of FH VLPs to stimulate BMDC maturation was much weaker than LPS (data not shown). The inability of FljB to significantly stimulate murine BMDC maturation was in line with previous report [31].

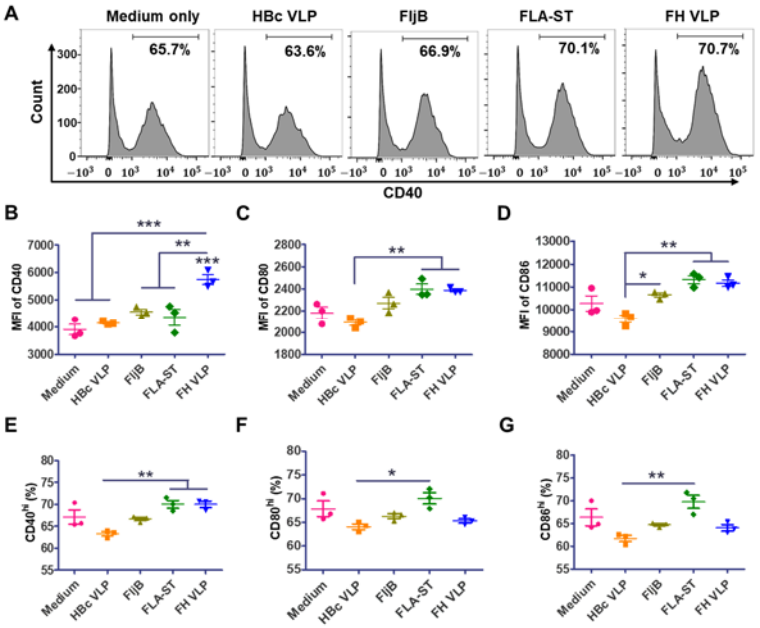

Fig.5 FH VLPs stimulate DC maturation *in vitro*

BMDCs were incubated with FljB, FLA-ST, HBc VLPs, and FH VLPs in triplicate at equal molar concentrations (70 nM). Cells were harvested 20 hours later and stained with fluorescence-conjugated anti-CD11c, CD86, CD80, CD40 antibodies followed by flow cytometry analysis. Cells were first gated based on SSC and FSC and then based on CD11c expression. $CD11c^{+}$ cells were analyzed for expression of CD40, CD80, and CD86. **A**. Representative histogram of CD40 expression and percentage of $CD40^{hi}$ DCs. **B-D**. MFI of CD40 (**B**), CD80 (**C**), and CD86 (**D**) in $CD11c^{+}$ DCs. **E-G**. Percentage of $CD40^{hi}$ (**E**), $CD80^{hi}$ (**F**), and $CD86^{hi}$ (**G**) in $CD11c^{+}$ DCs. One-way ANOVA with Bonferroni's multiple comparison test was used to compare differences between groups. *: $p<0.05$; **: $p<0.01$; ***: $p<0.001$. Experiments were repeated twice with similar results.

Next, we explored whether FH VLPs could also stimulate DC maturation *in vivo*. To explore this, C57BL/6 mice were intradermally injected with FH VLPs, FljB, and HBc VLPs. Skin was dissected 24 hours later for exploration of CD40, CD80, and CD86 expression on $CD11c^+$ DCs. As shown in Fig.6A-B, percentage of $CD40^{hi}$ cells in $CD11c^+$ DCs was significantly increased in FH VLP but not FljB or HBc VLP group when compared to that in PBS group. MFI of CD40 was also significantly increased in FH VLP but not FljB or HBc VLP group when compared to that in PBS group (Fig.6C). As *in intro* studies, no significant increase of MFI of CD80 or CD86 was found in FH VLPs, FljB, or HBc VLPs when compared to that in PBS group (Fig.6D-E). These results indicated FH VLPs could also significantly increase CD40 expression and stimulate DC maturation *in vivo*.

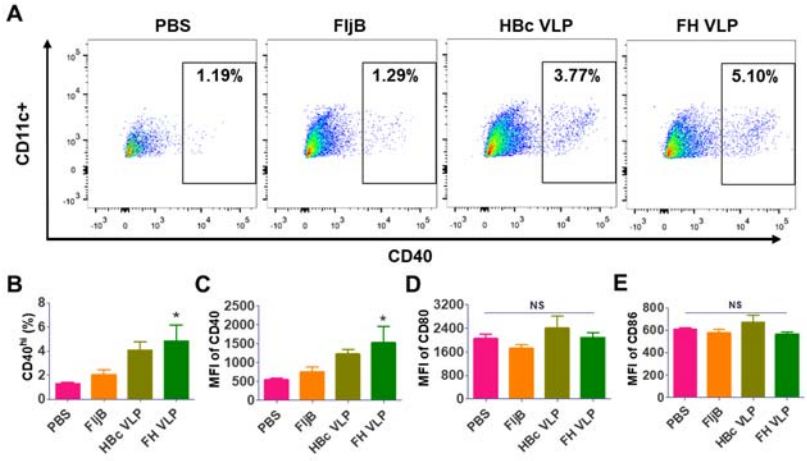

Fig.6 FH VLPs stimulate DC maturation *in vivo*

Lateral back skin of C57BL/6 mice was intradermally injected with 5 μg FH VLPs, 3.7 μg FljB, and 1.2 μg HBc VLPs (equal moles) in 20 μl or an equal volume of PBS to serve as control. Skin was dissected 24 hours later. Single-cell suspensions were prepared and stained with fluorescence-conjugated anti-CD11c, CD40, CD80, and CD86 antibodies followed by flow cytometry analysis. Cells were first gated based on FSC and SSC and then based on CD11c expression. $CD11c^+$ cells were analyzed for CD40, CD80, and CD86 expression. **A**. Representative dot plots showing percentage of $CD40^{hi}$ DCs. **B**. Comparison of percentage of $CD40^{hi}$ DCs among different groups. **C-E**. MFI of CD40 (**C**), CD80 (**D**), and CD86 (**E**) in $CD11c^+$ DCs. n=4. One-way ANOVA with Bonferroni's multiple comparison test was used to compare differences between groups. *: $p<0.05$; NS: not significant.

FH VLPs are more immunogenic than FljB

More efficient uptake and stimulation of DC maturation indicated FH VLPs might have improved immunogenicity as compared to FljB. To prove this, mice were immunized with FH VLPs and FljB (equal moles) and anti-FljB antibody responses were then measured and compared between groups. Flagellin was reported to mainly induce Th1-biased IgG1 antibody responses with high dependence on MyD88 [32, 33]. To explore FH VLP-induced antibody isotype and the dependence on MyD88, MyD88 KO mice were also included in above immunization studies. As shown in Fig.7A, FH VLPs induced 2.2-fold higher anti-FljB antibody titer than FljB. Lack of MyD88 almost completely abrogated FljB-induced antibody production but only partially inhibited FH VLP-induced anti-FljB antibody production (Fig.7A). FH VLP and FljB-induced isotype IgG1 and IgG2c antibody titer was also compared. As shown in

Fig.7B, FljB was found to induce strong IgG1 and weak IgG2c antibody titer, hinting the induction of Th2-biased antibody responses. Lack of MyD88 almost completely abrogated FljB-induced IgG1 and IgG2c antibody production (Fig.7B). In comparison, FH VLPs induced strong anti-FljB IgG2c and weak IgG1 antibody titer (Fig.7C), hinting the induction of Th1-biased antibody responses. Lack of MyD88 partially reduced FH VLP-induced IgG2c antibody production and showed no significant effects on FH VLP-induced IgG1 antibody production (Fig.7C). Due to the crucial role of IL-12 in skewing Th1-biased immune responses [34], we further measured IL-12 levels in BMDC stimulation studies and found FH VLPs but not FljB or FLA-ST stimulated significant IL-12 release (Suppl. Fig.5). This result at least partially explained strong induction of Th1-biased IgG2c antibody responses by FH VLPs. We further measured anti-HBc antibody titer and found FH VLPs failed to induce significant anti-HBc antibody production (Fig.7D), which was most likely due to the embedding of HBc in interior of FH VLPs. The above studies indicated FH VLPs were more immunogenic than FljB in stimulation of anti-FljB antibody production.

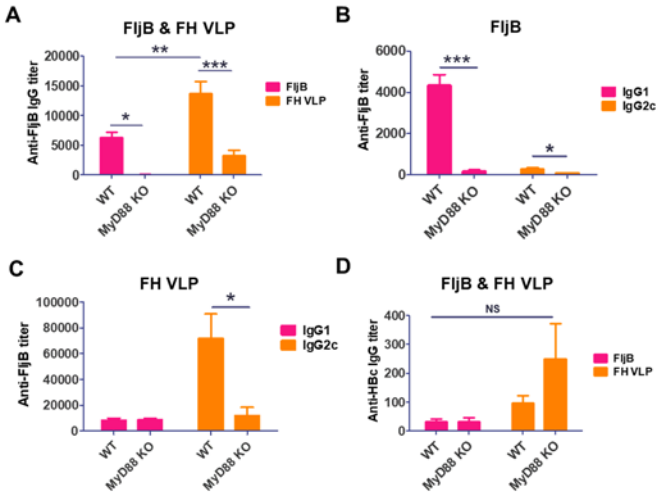

Fig.7 FH VLPs induce more potent anti-FljB antibody responses than FljB
WT and MyD88 KO mice were intradermally immunized with 5 μg FH VLPs or 3.7 μg FljB (equal moles). Immunization was repeated 3 weeks later. Serum antibody titer was measured 3 weeks after boost. **A**. Serum anti-FljB IgG antibody titer after FH VLP and FljB immunization. **B**. Serum anti-FljB IgG1 and IgG2c antibody titer after FljB immunization. **C**. Serum anti-FljB IgG1 and IgG2c antibody titer after FH VLP immunization. **D**. Serum anti-HBc IgG titer after FH VLP and FljB immunization. n=6. One-way ANOVA with Bonferroni's multiple comparison test was used to compare differences between groups. *, $p<0.05$; **, $p<0.01$; ***, $P<0.001$. NS: not significant.

Improved systemic safety of FH VLPs
Significantly reduced TLR5 activation ability implicated FH VLPs might have improved safety as compared to FljB. To prove this, we first measured serum IL-6 levels following FH VLP and FljB immunization of WT and MyD88 KO mice in above studies (Fig.7) considering IL-6 was linked to systemic adverse reactions of flagellin-based vaccines [12-15]. As shown in Fig.8A, serum IL-6 levels were significantly increased in WT mice at 6 hours after both FH VLP and FljB immunizations. Serum IL-6 levels returned to baseline levels 24 hours after FH VLP immunization and remained at relatively high levels 24 hours after FljB immunization in WT

mice (Fig.8B). This result indicated FH VLPs induced more transient systemic IL-6 release than FljB. Interestingly, serum IL-6 levels failed to significantly increase after FH VLP or FljB immunization in MyD88 KO mice (Fig.8A-B), hinting crucial roles of MyD88 in mediating FljB-induced systemic IL-6 release. The relative ability of FH VLPs and FljB to induce systemic IL-6 release was also explored in BALB/c mice. FljB was found to significantly increase serum IL-6 levels at 6 hours, while FH VLPs failed to significantly increase serum IL-6 levels at the same time (Fig.8C). Serum IL-6 levels reduced to baseline levels 24 hours after immunization in both groups (Fig.8D). These results indicated FH VLPs had significantly reduced ability to induce systemic IL-6 release than FljB.

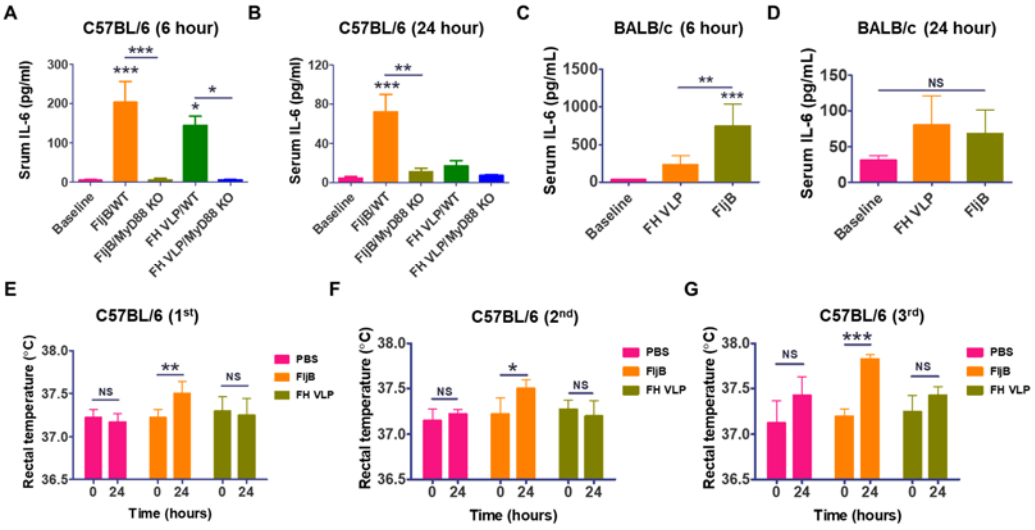

Fig.8 Significantly improved systemic safety of FH VLPs

A-B. Serum IL-6 levels were measured 6 (**A**) and 24 hours (**B**) after boost immunization of WT and MyD88 KO mice in Fig.7. Serum IL-6 levels before immunization was also measured (baseline). **C-D**. BALB/c mice were intradermally immunized with 5 μg FH VLPs or 3.7 μg FljB (equal moles). Immunization was repeated 3 weeks later. Serum IL-6 levels were measured just before boost immunization or 6 (**C**) and 24 hours (**D**) after boost immunization. **E-G**. C57BL/6 mice were intradermally immunized with 20 μg FH VLPs or 14.8 μg FljB (equal moles). Immunization was repeated weekly for 3 weeks. Rectal temperature was measured right before each immunization (0 hour) or 24 hours after each immunization. n=6 in **A-D** and n=4 in **E-G**. One-way ANOVA with Bonferroni's multiple comparison test was used to compare differences between groups in **A-D**. One-tailed student's t-test was used to compared differences between 0 and 24 hours within the same group in **E-G**. *, $p<0.05$; **, $p<0.01$; ***, $P<0.001$. NS: not significant.

Besides induction of systemic IL-6 release, flagellin-based vaccines also induced systemic adverse reactions, like fever, in clinical trials [12-15]. Next, we compared the ability of FH VLPs and FljB to induce fever-related systemic adverse reactions in murine models. To explore this, C57BL/6 mice were intradermally immunized with increased doses of FH VLPs and FljB (20 and 14.8 μg, respectively) weekly for 3 weeks and rectal temperature was measured right before and 24 hours after each immunization. Rectal temperature was measured with a mouse rectal temperature probe connected to PhysioSuite (Kent Scientific). Increase of FH VLP and Fljb doses in this study was because the previous FH VLP and FljB doses (5 and 3.7 μg, respectively) failed to significantly increase rectal temperature of mice (data not shown). As shown in Fig.8E-

G, FljB significantly increased rectal temperature by 0.275°C at 24 hours after the 1st and 2nd immunizations and increased rectal temperature by 0.625°C after the 3rd immunization. In contrast, FH VLPs failed to significantly increase rectal temperature after each immunization (Fig.7E-G). These data indicated FH VLPs had significantly reduced ability to increase rectal temperature of mice than FljB. We further found FH VLPs and FljB at the increased doses failed to induce microscopic tissue damage or body weight change as compared to PBS-injected mice (Fig.9), indicating the lack of systemic toxicity of both agents.

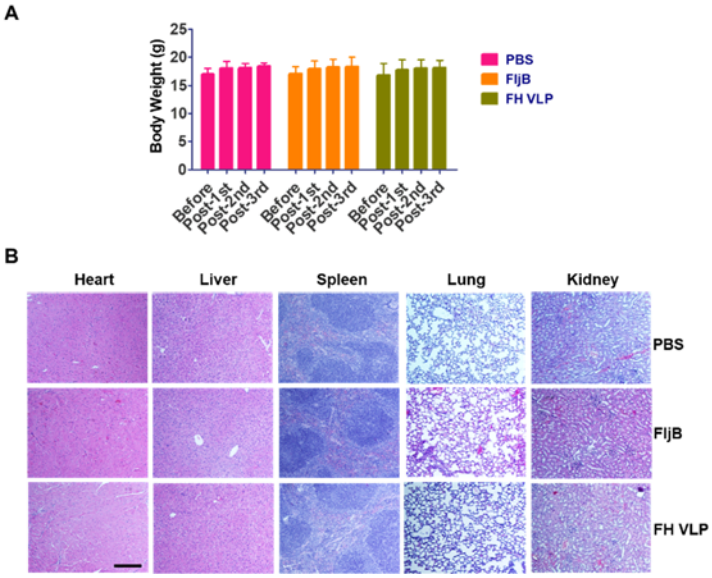

Fig.9 Lack of overt toxicity of FH VLPs

A. Body weight of C57BL/6 mice in Fig.7E-G was measured before immunization and one week after each immunization and compared among groups. **B**. Mice were sacrificed one week after the last immunization. Major organs, like heart, liver, spleen, lung, and kidney, were harvested, fixed in formalin, and then subjected to paraffin sectioning and H & E staining. Representative H & E-stained histological images were shown. Scale: 200 μm.

More immunogenic FH VLPs than FljB, HBc VLPs or KLH for nicotine vaccine development

The above studies indicated FH VLPs might be a more immunogenic and safer carrier than FljB for vaccine development. Next, nicotine vaccines were used as a model to compare relative immunogenicity and safety of FH VLPs to FljB, HBc VLPs, or the widely used KLH for nicotine vaccine development. Nicotine vaccines hold a great promise for anti-nicotine immunotherapy [35]. Despite the unsatisfied clinical outcomes of several nicotine vaccines (NicVAX, NicQb, Niccine) [35-37], different strategies are under exploration to improve anti-nicotine immunotherapy that include improved vaccine carriers [25, 38-45]. KLH was found to be a more immunogenic carrier than recombinant Pseudomonas Exoprotein A (rEPA) used in NicVAX for nicotine vaccine development [46]. Flagellin (FliC) was also explored as both vaccine carriers and adjuvants for nicotine vaccine development [47]. FliC-based nicotine vaccine was found to induce anti-nicotine antibodies with superior nicotine binding to Tetanus Toxoid (TT)-based nicotine vaccine [47]. Here, we first compared relative immunogenicity of KLH to FljB and HBc VLPs for nicotine vaccine development. As shown in Suppl. Fig.6A, KLH-Nic elicited ~2 times higher anti-nicotine antibody (NicAb) titer than FljB-Nic. In another study, we compared relative immunogenicity of KLH-Nic and HBc-Nic and found KLH-Nic elicited ~5 times higher NicAb

titer than HBc-Nic (Suppl. Fig.6B). These studies indicated KLH was more immunogenic than FljB and HBc VLPs for nicotine vaccine development.

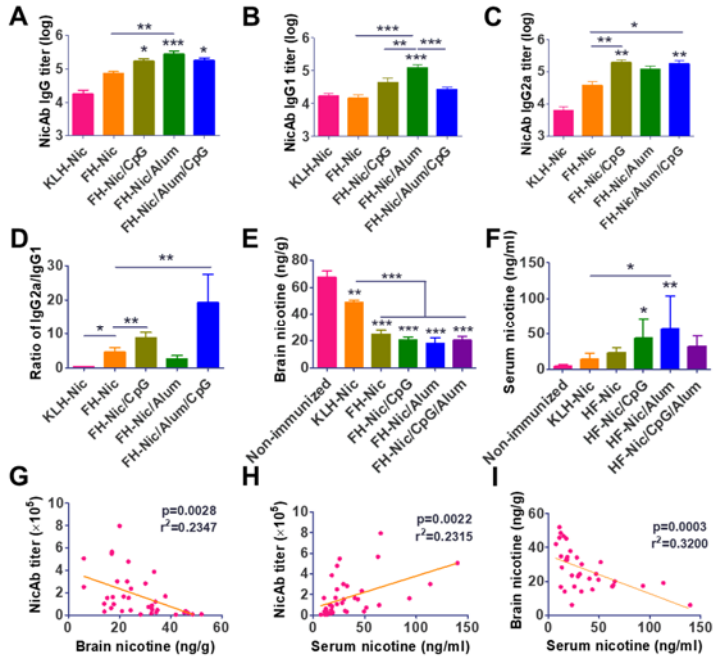

Fig.10 High immunogenicity of FH VLPs for nicotine vaccine development
BALB/c mice were intradermally immunized with KLH-Nic, FH-Nic, or FH-Nic in the presence of CpG, Alum, or CpG/Alum adjuvant for total 3 times with a 3-week interval. Serum NicAb titer was measured 3 weeks after the last immunization. Mice were then intravenously challenged with 0.03 mg/kg nicotine within one week after the last blood collection to measure serum NicAb titer. Five minutes later, brain and serum samples were isolated for quantification of tissue nicotine levels. **A-D**. Total IgG titer was shown in **A** and subtype IgG1 and IgG2a antibody titer was shown in **B** & **C**, respectively. Ratio of IgG2a to IgG1 antibody titer was shown in **D**. **E-F**. Brain (**E**) and serum nicotine levels (**F**) of different groups. **G-I.** Data of all groups were pooled for linear correlation analysis between NicAb titer and brain nicotine levels (**G**), brain and serum nicotine levels (**H**), and NicAb titer and serum nicotine levels (**I**). n=6-8 per group. One-way ANOVA with Tukey's Multiple Comparison Test was used to compare differences between groups in **B** and **D**. One-way ANOVA with Newman-Keuls Multiple Comparison Test was used to compare differences between groups in **A** and **C**. One-way ANOVA with Tukey's Multiple Comparison Test was used to compare differences between groups in **E**. One-way ANOVA with Newman-Keuls Multiple Comparison Test was used to compare differences between groups in **F**. *: $p<0.05$; **: $p<0.01$; ***: $p<0.001$.

Next, we compared relative immunogenicity of FH-Nic to KLH-Nic. Due to the synergy between two of the three adjuvants (FljB, CpG, and Alum) [48-50], we also evaluated whether incorporation of CpG, Alum, or combinatorial CpG/Alum adjuvant could increase immunogenicity of FH-Nic. As shown in Fig.10A, FH-Nic elicited more than 4 times higher NicAb titer than KLH-Nic. Incorporation of CpG or Alum adjuvant further increased NicAb titer by 2.3 and 3.8 times, respectively, while incorporation of CpG/Alum adjuvant failed to further increase NicAb titer as compared to incorporation of either adjuvant alone (Fig.10A). Antibody isotype analysis found FH-Nic mainly increased anti-nicotine IgG2a but not IgG1 antibody titer

as compared to KLH-Nic (Fig.10B-C). Incorporation of Th1 adjuvant CpG and Th2 adjuvant Alum increased anti-nicotine IgG2a and IgG1 titer, respectively (Fig.10B-C). In line with these data, anti-nicotine IgG2a/IgG1 ratio was increased after incorporation of CpG adjuvant and reduced after incorporation of Alum adjuvant (Fig.10D). Besides antibody titer, we also evaluated antibody avidity index due to its importance in sequestration of nicotine in the peripheral tissue. As shown in Suppl. Fig.7, similar antibody avidity index was observed between KLH-Nic and FH-Nic groups. Incorporation of Alum or CpG adjuvant into FH-Nic vaccination increased antibody avidity to a statistically non-significant level. Interestingly, incorporation of combinatorial CpG/Alum adjuvant failed to increase antibody avidity as compared to FH-Nic vaccination alone (Suppl. Fig.7).

Mice were further challenged with intravenous nicotine and brain and blood were collected 5 minutes later to quantify tissue nicotine levels. As compared to brain nicotine levels of non-immunized mice, KLH-Nic immunization reduced brain nicotine levels by 27% and FH-Nic immunization reduced brain nicotine levels by 63% (Fig.10E). Incorporation of Alum or CpG adjuvant into FH-Nic immunization reduced brain nicotine levels by 74% and 69%, respectively (Fig.10E). Incorporation of CpG/Alum adjuvant into FH-immunization reduced brain nicotine levels by 70%, similar to incorporation of CpG adjuvant alone (Fig.10E). Serum nicotine levels showed an opposite trend to brain nicotine levels with relatively big variations within groups (Fig.10F), in line with other report [51]. Data of all groups were pooled for linear correlation analysis. A negative correlation was identified between serum NicAb titer and brain nicotine levels (Fig.10G) and between brain and serum nicotine levels (Fig.10H), while a positive correlation was found between serum NicAb titer and serum nicotine levels (Fig.10I). The negative correlation between serum NicAb titer and brain nicotine levels supports the generation of high NicAb titer to block nicotine entry into the brain. Lastly, we explored local and systemic safety of ID FH-Nic immunization. As shown in Suppl. Fig.8A, ID FH-Nic induced minimal local reactions as supported by the lack of visible changes of FH-Nic-injected skin. ID FH-Nic also failed to induce significant systemic reactions as supported by the baseline levels of serum IL-6 at 6 and 24 hours after immunization (Suppl. Fig.8B).

Discussion

This study explored high-density display of flagellin on HBc VLP surface to improve its immunogenicity and safety as vaccine carriers. High-density FljB-displayed HBc VLPs or FH VLPs were prepared by insertion of full-length FljB into c/e1 loop of HBc followed by *E. Coli* expression and self-assembly. Due to the small size of HBc VLPs, insertion of full-length proteins poses a significant risk to interfere with self-assembly of HBc into VLPs. To our knowledge, only two full-length proteins (GFP and OspC) less than 250 aa were successfully displayed on HBc VLP surface upon c/e1 loop insertion [20, 21]. This study may be the first to describe full-length protein of more than 500 aa could be inserted into c/e1 loop of HBc for successful display on HBc VLP surface. Close juxtaposition of N- and C-termini of FljB is expected to be crucial for the successful display of FljB on HBc VLP surface. The elongated D0/D1 domain of FljB may also be important considering the unique structure poses little steric hindrance to self-assembly of FH VLPs. Flagellin has been also chemically conjugated to HBc VLPs [52, 53]. In those studies, only a small fraction of HBc molecules were conjugated with flagellin [52, 53]. Low-density display of flagellin on HBc VLP surface was found not to significantly impact its TLR5 activation ability [53]. Besides HBc VLPs, flagellin was also displayed on influenza Matrix 1 (M1) VLP surface by co-expression of membrane-anchored flagellin and M1 in insect cells [54, 55]. The content of flagellin in M1 VLPs was found to be about 1.3% or 8% of total protein [54, 55]. Low-density display of flagellin on M1 VLPs showed comparable TLR5 activation ability to free flagellin [54]. Different from these strategies that resulted in low-density display of flagellin on VLP surface, self-assembly of FljB-HBc fusion protein led to high-density display of FljB onto HBc VLP surface with ~80% flagellin content. High-density display of FljB on HBc VLP surface also showed at least 100-fold reduced TLR5 activation ability as compared to FljB (Fig.2A). Besides significantly reduced TLR5 activation ability, FH VLPs also lost most of its NLRC4 inflammasome and Caspase 1 activation ability (Fig.2B). D0/D1 domains of FljB, crucial for TLR5 and NLRC4 inflammasome activation, were likely buried in interior of FH VLPs without access to TLR5 or NLRC4 inflammasome. In support, self-assembly of flagellin into flagella filaments also lost most of the TLR5 activation ability due to the embedding of D0/D1 domain of flagellin in interior of flagella filaments [4]. Yet, our study cannot exclude the possibility that partially impaired folding of D0/D1 domains of FljB also contributed to the significant reduction of TLR5 and NLRC4 inflammasome activation ability of FH VLPs. Despite significant reduction of TLR5 activation ability, FH VLPs showed similar adjuvant effects to boost co-administered OVA immunization to FljB (Fig.2C-D). This result indicated adjuvant effects of flagellin could be maintained even with a significant loss of TLR5 activation ability, in line with previous report [11]. Also, FH VLPs induced more than 2-fold anti-FljB antibody titer than FljB, indicating improved immunogenicity (Fig.7A).

Interestingly, FH VLPs mainly induced anti-FljB IgG2c antibody titer, while FljB mainly induced anti-FljB IgG1 antibody titer (Fig.7B-C). Induction of Th1-biased IgG2a antibody responses was also reported by influenza M1 VLP-displayed flagellin at relatively low densities [54, 55]. These data indicate induction of strong anti-FljB IgG2 antibody responses may be the common feature of VLP-displayed flagellin regardless of high- or low-density display. Induction of strong IgG2 antibody responses was in line with our observation that FH VLPs but not FljB induced BMDCs to secret high levels of IL-12, which is a key cytokine to induce Th1-skewing immune responses [34]. Significant reduction of IgG2c antibody titer in MyD88 KO mice (Fig.7C) indicated crucial roles of MyD88 in FH VLP-induced IgG2c antibody production. Yet,

significant IgG2c antibody titer was still induced in the absence of MyD88 (Fig.7C), indicating FH VLPs also activated other signaling pathways to mediate IgG2c antibody production. FH VLPs failed to induce significant anti-HBc antibody production due to the embedding of HBc in interior of FH VLPs (Fig.7D). The high immunogenicity of FH VLPs could be explained by its increased uptake by APCs and induction of stronger DC maturation than FljB (Fig.4-6, Suppl. Fig.4). The increased uptake of FH VLPs may simply reflect more efficient uptake of particulate antigens by phagocytosis than soluble antigen uptake by non-receptor-mediated endocytosis (macropinocytosis) [56]. Increased uptake of FH VLPs may also be mediated by cell surface receptors. Although murine BMDCs don't express TLR5 [31], we cannot exclude the possibility of other cell surface receptors, such as glycolipids/gangliosides (e.g., asialo-GM1, GM1, GD1a) and lipid rafts [57], that more efficiently bind high-density displayed FljB than soluble FljB, leading to more efficient uptake of FH VLPs than FljB. Our studies found FH VLPs specifically increased CD40 expression on DC surface with no significant effects on CD80 and CD86 expression (Fig.5-6). All the other stimuli, like FljB, FLA-ST, and HBc VLPs, showed no significant effects on CD40, CD80, or CD86 expression on DC surface (Fig.5-6).

Using nicotine vaccine as a model, we compared relative immunogenicity of FH VLPs to FljB, HBc VLPs, and widely used KLH for nicotine vaccine development. FH VLPs were found to be a more immunogenic carrier than the widely used KLH and KLH was more immunogenic than FljB and HBc VLPs for nicotine vaccine development (Fig.10A, Suppl. Fig.6). FH-Nic immunization induced ~4 times higher NicAb titer and more significant inhibited nicotine entry into the brain than KLH-Nic immunization (Fig.10A & E). Few studies directly compared relative immunogenicity of FljB to KLH for vaccine development. Lockner et al. found FliC-based cocaine vaccine elicited comparable anti-cocaine hapten antibody titer to KLH-based cocaine vaccine in the presence of Alum adjuvant [48]. In consideration of potential synergy between Alum and FliC, immunogenicity of FliC for cocaine vaccine development might be weaker than KLH, consistent with the observation in our nicotine vaccine development studies. We found incorporation of Alum or CpG adjuvant into FH-Nic immunization could further increase NicAb production and reduce nicotine entry into the brain after nicotine challenge (Fig.10A & E). Interestingly, incorporation of CpG/Alum adjuvant failed to further increase NicAb production and yet induced more Th1-biased immune responses (Fig.10A & D). These results indicated no advantages to incorporate both Alum and CpG adjuvants to boost FH-Nic-induced antibody responses.

Besides high immunogenicity, FH VLPs showed a good system safety. FH VLPs induced more transient systemic IL-6 release than FljB in C57BL/6 mice and FH VLPs failed to significantly increase serum IL-6 levels in BALB/c mice (Fig.8A-D). Furthermore, FH VLPs failed to increase rectal temperature of mice even after repeated administrations at relatively high doses, while soluble FljB at an equivalent dose consistently and significantly increased rectal temperature of mice (Fig.8E-G). No significant microscopic organ damage or body weight change relative to control group was observed following FH VLP immunization (Fig.9). These results indicated FH VLPs had improved systemic safety than FljB.

VLPs are self-assembled nanostructures, mimicking the size and shape of infectious viruses, and can be used as vaccines alone. VLP-based hepatitis b vaccine and human papillomavirus vaccine have been approved for human use [22]. VLPs are also highly attractive vaccine carriers and can

be engineered to express foreign antigens to elicit potent immune responses [58]. High-density display of FljB on HBc VLP surface generates a new VLP delivery platform (FH VLPs) with good immunogenicity and safety for vaccine development. This study found FH VLPs to be a highly immunogenic carrier for conjugate vaccine development. Besides conjugate vaccines, antigenic epitopes can be inserted into the flexible D3 domain of FljB for high-density display of FH VLP surface. Even full-length proteins may be inserted into D3 domain or replace D3 domain for high-density display on FH VLP surface. Thus, FH VLPs may provide a more versatile delivery platform than HBc VLPs considering c/e1 loop of HBc only allows insertion of relatively short antigenic epitopes and D3 domain of flagellin allows insertion of foreign antigens with less restriction on lengths and 3D structures. FljB-HBc fusion proteins can be conveniently expressed in *E. Coli* in large scale and refolded *in vitro* to form VLPs. The superior immunogenicity, good safety, and large-scale production support further development of FH VLPs to use as vaccine carriers.

Acknowledgements
This work is partly supported by the National Institutes of Health grants DA033371 and AI139473 (to X.Y.C.). Microplate reader, BD FACSVerse, EVOS Cell Imaging System, and Jasco 1100 CD Spectropolarimeter used in this work are supported by an Institutional Development Award (IDeA) from the National Institute of General Medical Sciences of the National Institutes of Health grant P20GM103430. TEM images were captured at RI Consortium for Nanoscience and Nanotechnology Lab supported by the National Science Foundation (NSF) EPSCoR Cooperative Agreement #OIA-1655221. Histological work reported in this publication was supported by the Molecular Pathology Core of the COBRE Center for Cancer Research Development, funded by the National Institute of General Medical Sciences of the National Institutes of Health under Award Number P30GM110759.

Data Availability
The raw/processed data required to reproduce these findings are available from the corresponding author upon request.

References

[1] K. Yonekura, S. Maki-Yonekura, K. Namba, Complete atomic model of the bacterial flagellar filament by electron cryomicroscopy, Nature 424(6949) (2003) 643-50.
[2] F. Hayashi, K.D. Smith, A. Ozinsky, T.R. Hawn, E.C. Yi, D.R. Goodlett, J.K. Eng, S. Akira, D.M. Underhill, A. Aderem, The innate immune response to bacterial flagellin is mediated by Toll-like receptor 5, Nature 410(6832) (2001) 1099-103.
[3] Y. Zhao, J. Yang, J. Shi, Y.N. Gong, Q. Lu, H. Xu, L. Liu, F. Shao, The NLRC4 inflammasome receptors for bacterial flagellin and type III secretion apparatus, Nature 477(7366) (2011) 596-600.
[4] K.D. Smith, E. Andersen-Nissen, F. Hayashi, K. Strobe, M.A. Bergman, S.L. Barrett, B.T. Cookson, A. Aderem, Toll-like receptor 5 recognizes a conserved site on flagellin required for protofilament formation and bacterial motility, Nature immunology 4(12) (2003) 1247-53.
[5] W.S. Song, Y.J. Jeon, B. Namgung, M. Hong, S.I. Yoon, A conserved TLR5 binding and activation hot spot on flagellin, Scientific reports 7 (2017) 40878.
[6] E.F. Halff, C.A. Diebolder, M. Versteeg, A. Schouten, T.H. Brondijk, E.G. Huizinga, Formation and structure of a NAIP5-NLRC4 inflammasome induced by direct interactions with conserved N- and C-terminal regions of flagellin, The Journal of biological chemistry 287(46) (2012) 38460-72.
[7] M. Vijay-Kumar, F.A. Carvalho, J.D. Aitken, N.H. Fifadara, A.T. Gewirtz, TLR5 or NLRC4 is necessary and sufficient for promotion of humoral immunity by flagellin, European journal of immunology 40(12) (2010) 3528-34.
[8] I.A. Hajam, P.A. Dar, I. Shahnawaz, J.C. Jaume, J.H. Lee, Bacterial flagellin-a potent immunomodulatory agent, Experimental & molecular medicine 49(9) (2017) e373.
[9] H.R. Bonifield, K.T. Hughes, Flagellar phase variation in Salmonella enterica is mediated by a posttranscriptional control mechanism, Journal of bacteriology 185(12) (2003) 3567-74.
[10] T. Ben-Yedidia, R. Arnon, Effect of pre-existing carrier immunity on the efficacy of synthetic influenza vaccine, Immunology letters 64(1) (1998) 9-15.
[11] C.J. Sanders, L. Franchi, F. Yarovinsky, S. Uematsu, S. Akira, G. Nunez, A.T. Gewirtz, Induction of adaptive immunity by flagellin does not require robust activation of innate immunity, European journal of immunology 39(2) (2009) 359-71.
[12] J.J. Treanor, D.N. Taylor, L. Tussey, C. Hay, C. Nolan, T. Fitzgerald, G. Liu, U. Kavita, L. Song, I. Dark, A. Shaw, Safety and immunogenicity of a recombinant hemagglutinin influenza-flagellin fusion vaccine (VAX125) in healthy young adults, Vaccine 28(52) (2010) 8268-74.
[13] C.B. Turley, R.E. Rupp, C. Johnson, D.N. Taylor, J. Wolfson, L. Tussey, U. Kavita, L. Stanberry, A. Shaw, Safety and immunogenicity of a recombinant M2e-flagellin influenza vaccine (STF2.4xM2e) in healthy adults, Vaccine 29(32) (2011) 5145-52.
[14] D.N. Taylor, J.J. Treanor, E.A. Sheldon, C. Johnson, S. Umlauf, L. Song, U. Kavita, G. Liu, L. Tussey, K. Ozer, T. Hofstaetter, A. Shaw, Development of VAX128, a recombinant hemagglutinin (HA) influenza-flagellin fusion vaccine with improved safety and immune response, Vaccine 30(39) (2012) 5761-9.
[15] L. Tussey, C. Strout, M. Davis, C. Johnson, G. Lucksinger, S. Umlauf, L. Song, G. Liu, K. Abraham, C.J. White, Phase 1 Safety and Immunogenicity Study of a Quadrivalent Seasonal Flu Vaccine Comprising Recombinant Hemagglutinin-Flagellin Fusion Proteins, Open forum infectious diseases 3(1) (2016) ofw015.

[16] S.B. Mizel, J.T. Bates, Flagellin as an adjuvant: cellular mechanisms and potential, Journal of immunology (Baltimore, Md. : 1950) 185(10) (2010) 5677-82.
[17] U. Arora, P. Tyagi, S. Swaminathan, N. Khanna, Chimeric Hepatitis B core antigen virus-like particles displaying the envelope domain III of dengue virus type 2, Journal of nanobiotechnology 10 (2012) 30.
[18] I. Sominskaya, D. Skrastina, A. Dislers, D. Vasiljev, M. Mihailova, V. Ose, D. Dreilina, P. Pumpens, Construction and immunological evaluation of multivalent hepatitis B virus (HBV) core virus-like particles carrying HBV and HCV epitopes, Clinical and vaccine immunology : CVI 17(6) (2010) 1027-33.
[19] K. Roose, S. De Baets, B. Schepens, X. Saelens, Hepatitis B core-based virus-like particles to present heterologous epitopes, Expert review of vaccines 12(2) (2013) 183-98.
[20] P.A. Kratz, B. Bottcher, M. Nassal, Native display of complete foreign protein domains on the surface of hepatitis B virus capsids, Proceedings of the National Academy of Sciences of the United States of America 96(5) (1999) 1915-20.
[21] C. Skamel, M. Ploss, B. Bottcher, T. Stehle, R. Wallich, M.M. Simon, M. Nassal, Hepatitis B virus capsid-like particles can display the complete, dimeric outer surface protein C and stimulate production of protective antibody responses against Borrelia burgdorferi infection, The Journal of biological chemistry 281(25) (2006) 17474-81.
[22] N. Kushnir, S.J. Streatfield, V. Yusibov, Virus-like particles as a highly efficient vaccine platform: diversity of targets and production systems and advances in clinical development, Vaccine 31(1) (2012) 58-83.
[23] X. Chen, Q. Zeng, M.X. Wu, Improved efficacy of dendritic cell-based immunotherapy by cutaneous laser illumination, Clinical cancer research : an official journal of the American Association for Cancer Research 18(8) (2012) 2240-9.
[24] Y. Cao, X. Zhu, M.N. Hossen, P. Kakar, Y. Zhao, X. Chen, Augmentation of vaccine-induced humoral and cellular immunity by a physical radiofrequency adjuvant, Nature communications 9(1) (2018) 3695.
[25] X. Chen, M. Pravetoni, B. Bhayana, P.R. Pentel, M.X. Wu, High immunogenicity of nicotine vaccines obtained by intradermal delivery with safe adjuvants, Vaccine 31(1) (2012) 159-64.
[26] P.R. Pentel, D.H. Malin, S. Ennifar, Y. Hieda, D.E. Keyler, J.R. Lake, J.R. Milstein, L.E. Basham, R.T. Coy, J.W. Moon, R. Naso, A. Fattom, A nicotine conjugate vaccine reduces nicotine distribution to brain and attenuates its behavioral and cardiovascular effects in rats, Pharmacol Biochem Behav 65(1) (2000) 191-8.
[27] R.A. Macdonald, C.S. Hosking, C.L. Jones, The measurement of relative antibody affinity by ELISA using thiocyanate elution, Journal of immunological methods 106(2) (1988) 191-4.
[28] P.T. Wingfield, S.J. Stahl, R.W. Williams, A.C. Steven, Hepatitis core antigen produced in Escherichia coli: subunit composition, conformational analysis, and in vitro capsid assembly, Biochemistry 34(15) (1995) 4919-32.
[29] C.A. Scarff, M.J.G. Fuller, R.F. Thompson, M.G. Iadaza, Variations on Negative Stain Electron Microscopy Methods: Tools for Tackling Challenging Systems, Journal of visualized experiments : JoVE (132) (2018).
[30] J.S. Blum, P.A. Wearsch, P. Cresswell, Pathways of antigen processing, Annual review of immunology 31 (2013) 443-73.

[31] T.K. Means, F. Hayashi, K.D. Smith, A. Aderem, A.D. Luster, The Toll-like receptor 5 stimulus bacterial flagellin induces maturation and chemokine production in human dendritic cells, Journal of immunology (Baltimore, Md. : 1950) 170(10) (2003) 5165-75.
[32] K. Smith, A. Lopez-Yglesias, C. Lu, X. Zhao, R. Strong, Flagellin's hypervariable D2/D3 domain is required for robust anti-flagellin primary antibody responses (VAC11P.1065), The Journal of Immunology 194(1 Supplement) (2015) 212.5-212.5.
[33] A. Didierlaurent, I. Ferrero, L.A. Otten, B. Dubois, M. Reinhardt, H. Carlsen, R. Blomhoff, S. Akira, J.P. Kraehenbuhl, J.C. Sirard, Flagellin promotes myeloid differentiation factor 88-dependent development of Th2-type response, Journal of immunology (Baltimore, Md. : 1950) 172(11) (2004) 6922-30.
[34] C. Heufler, F. Koch, U. Stanzl, G. Topar, M. Wysocka, G. Trinchieri, A. Enk, R.M. Steinman, N. Romani, G. Schuler, Interleukin-12 is produced by dendritic cells and mediates T helper 1 development as well as interferon-gamma production by T helper 1 cells, European journal of immunology 26(3) (1996) 659-68.
[35] T. Raupach, P.H. Hoogsteder, C.P. Onno van Schayck, Nicotine vaccines to assist with smoking cessation: current status of research, Drugs 72(4) (2012) e1-16.
[36] S. Tonstad, E. Heggen, H. Giljam, P.A. Lagerback, P. Tonnesen, L.D. Wikingsson, N. Lindblom, S. de Villiers, T.H. Svensson, K.O. Fagerstrom, Niccine(R), a nicotine vaccine, for relapse prevention: a phase II, randomized, placebo-controlled, multicenter clinical trial, Nicotine & tobacco research : official journal of the Society for Research on Nicotine and Tobacco 15(9) (2013) 1492-501.
[37] P.R. Pentel, M.G. LeSage, New directions in nicotine vaccine design and use, Advances in pharmacology (San Diego, Calif.) 69 (2014) 553-80.
[38] D.C. Pryde, L.H. Jones, D.P. Gervais, D.R. Stead, D.C. Blakemore, M.D. Selby, A.D. Brown, J.W. Coe, M. Badland, D.M. Beal, R. Glen, Y. Wharton, G.J. Miller, P. White, N. Zhang, M. Benoit, K. Robertson, J.R. Merson, H.L. Davis, M.J. McCluskie, Selection of a novel anti-nicotine vaccine: influence of antigen design on antibody function in mice, PloS one 8(10) (2013) e76557.
[39] J.W. Lockner, J.M. Lively, K.C. Collins, J.C. Vendruscolo, M.R. Azar, K.D. Janda, A conjugate vaccine using enantiopure hapten imparts superior nicotine-binding capacity, Journal of medicinal chemistry 58(2) (2015) 1005-11.
[40] K.E. Cornish, S.H. de Villiers, M. Pravetoni, P.R. Pentel, Immunogenicity of individual vaccine components in a bivalent nicotine vaccine differ according to vaccine formulation and administration conditions, PloS one 8(12) (2013) e82557.
[41] S.H. de Villiers, K.E. Cornish, A.J. Troska, M. Pravetoni, P.R. Pentel, Increased efficacy of a trivalent nicotine vaccine compared to a dose-matched monovalent vaccine when formulated with alum, Vaccine 31(52) (2013) 6185-93.
[42] Y. Hu, H. Zheng, W. Huang, C. Zhang, A novel and efficient nicotine vaccine using nano-lipoplex as a delivery vehicle, Human vaccines & immunotherapeutics 10(1) (2014) 64-72.
[43] H. Zheng, Y. Hu, W. Huang, S. de Villiers, P. Pentel, J. Zhang, H. Dorn, M. Ehrich, C. Zhang, Negatively Charged Carbon Nanohorn Supported Cationic Liposome Nanoparticles: A Novel Delivery Vehicle for Anti-Nicotine Vaccine, Journal of biomedical nanotechnology 11(12) (2015) 2197-210.
[44] Y. Hu, D. Smith, E. Frazier, R. Hoerle, M. Ehrich, C. Zhang, The next-generation nicotine vaccine: a novel and potent hybrid nanoparticle-based nicotine vaccine, Biomaterials 106 (2016) 228-39.

[45] R.I. Desai, J. Bergman, Effects of the Nanoparticle-Based Vaccine, SEL-068, on Nicotine Discrimination in Squirrel Monkeys, Neuropsychopharmacology : official publication of the American College of Neuropsychopharmacology 40(9) (2015) 2207-16.
[46] P.T. Bremer, K.D. Janda, Conjugate Vaccine Immunotherapy for Substance Use Disorder, Pharmacological reviews 69(3) (2017) 298-315.
[47] N.T. Jacob, J.W. Lockner, J.E. Schlosburg, B.A. Ellis, L.M. Eubanks, K.D. Janda, Investigations of Enantiopure Nicotine Haptens Using an Adjuvanting Carrier in Anti-Nicotine Vaccine Development, Journal of medicinal chemistry 59(6) (2016) 2523-9.
[48] J.W. Lockner, L.M. Eubanks, J.L. Choi, J.M. Lively, J.E. Schlosburg, K.C. Collins, D. Globisch, R.J. Rosenfeld-Gunn, I.A. Wilson, K.D. Janda, Flagellin as carrier and adjuvant in cocaine vaccine development, Molecular pharmaceutics 12(2) (2015) 653-62.
[49] C.L. Brazolot Millan, R. Weeratna, A.M. Krieg, C.A. Siegrist, H.L. Davis, CpG DNA can induce strong Th1 humoral and cell-mediated immune responses against hepatitis B surface antigen in young mice, Proceedings of the National Academy of Sciences of the United States of America 95(26) (1998) 15553-8.
[50] L. Sfondrini, A. Rossini, D. Besusso, A. Merlo, E. Tagliabue, S. Menard, A. Balsari, Antitumor activity of the TLR-5 ligand flagellin in mouse models of cancer, Journal of immunology (Baltimore, Md. : 1950) 176(11) (2006) 6624-30.
[51] V. Arutla, J. Leal, X. Liu, S. Sokalingam, M. Raleigh, A. Adaralegbe, L. Liu, P.R. Pentel, S.M. Hecht, Y. Chang, Prescreening of Nicotine Hapten Linkers in Vitro To Select Hapten-Conjugate Vaccine Candidates for Pharmacokinetic Evaluation in Vivo, ACS combinatorial science 19(5) (2017) 286-298.
[52] Y. Lu, J.P. Welsh, W. Chan, J.R. Swartz, Escherichia coli-based cell free production of flagellin and ordered flagellin display on virus-like particles, Biotechnol Bioeng 110(8) (2013) 2073-85.
[53] Y. Lu, J.R. Swartz, Functional properties of flagellin as a stimulator of innate immunity, Scientific reports 6 (2016) 18379.
[54] B.Z. Wang, F.S. Quan, S.M. Kang, J. Bozja, I. Skountzou, R.W. Compans, Incorporation of membrane-anchored flagellin into influenza virus-like particles enhances the breadth of immune responses, Journal of virology 82(23) (2008) 11813-23.
[55] E.J. Ko, Y. Lee, Y.T. Lee, Y.J. Jung, V.L. Ngo, M.C. Kim, K.H. Kim, B.Z. Wang, A.T. Gewirtz, S.M. Kang, Flagellin-expressing virus-like particles exhibit adjuvant effects on promoting IgG isotype-switched long-lasting antibody induction and protection of influenza vaccines in CD4-deficient mice, Vaccine 37(26) (2019) 3426-3434.
[56] C.M. Snapper, Distinct Immunologic Properties of Soluble Versus Particulate Antigens, Frontiers in immunology 9 (2018) 598.
[57] J. Haiko, B. Westerlund-Wikstrom, The role of the bacterial flagellum in adhesion and virulence, Biology 2(4) (2013) 1242-67.
[58] K.M. Frietze, D.S. Peabody, B. Chackerian, Engineering virus-like particles as vaccine platforms, Curr Opin Virol 18 (2016) 44-9.